Inorg. Chem. **2008**, *47*, 11202−11211

Probing Single-Chain Magnets in a Family of Linear Chain Compounds Constructed by Magnetically Anisotropic Metal-Ions and Cyclohexane-1,2-Dicarboxylate Analogues

Yan-Zhen Zheng,[†] Wei Xue,[†] Ming-Liang Tong,*[,†] Xiao-Ming Chen,*[,†] and Shao-Liang Zheng[‡]

MOE Key Laboratory of Bioinorganic and Synthetic Chemistry, School of Chemistry and Chemical Engineering, Sun Yat-Sen University, Guangzhou 510275, China, and Department of Chemistry, State University of New York at Buffalo, Buffalo, New York 14260-3000

Received August 7, 2008

Five new metal-carboxylate chain-based laminated compounds, namely, $^{2}_{\infty}$[Fe^{II}(*e,e-trans*-1,2-chdc)] (**3**) (1,2-chdc = cyclohexane-1,2-dicarboxylate), $^{2}_{\infty}$[Ni^{II}(μ-OH$_2$)(*e,a-cis*-1,2-chdc)] (**4**), $^{2}_{\infty}$[Co^{II}(μ-OH$_2$)(1,2-chedc)] (**5**) (1,2-chedc = cyclohex-1-ene-1,2-dicarboxylate), $^{2}_{\infty}$[Co$_5^{II}$(μ_3-OH)$_2$(OH$_2$)$_2$(1,2-chedc)$_4$] (**6**), and $^{2}_{\infty}$[Co^{II}(4-Me-1,2-chdc)] (**7**) (4-Me-1,2-chdc = *trans*-4-methylcyclohexane-1,2-dicarboxylate) have been hydrothermally synthesized. In these series of magnetic chain-based compounds, **3** and **7** have the same dimeric paddle-wheel M(II)-carboxylate chain as the previously reported compound, $^{2}_{\infty}$[Co^{II}(*trans*-1,2-chdc)] (**2**). However, compound **3** does not behave as a single-chain magnet (SCM) but simply an alternating ferro-antiferro magnetic chain. Compound **4** has the *cis* conformation of 1,2-chdc ligand, which leads to a uniform aqua-carboxylate-bridged Ni(II) chain. Such a Ni—O chain exhibits strong antiferromagnetic interactions, leading to a diamagnetic ground state. Compound **5** features a corner-sharing triangular chain, or Δ-chain, which is part of a Kagomé lattice. However, **5** does not exhibit a spin-frustrated effect but simply spin competition. Compound **6** has a unique pentanuclear Co^{II} cluster, which is further connected by the syn-anti carboxylate into a chain structure. Compound **6** exhibits antiferromagnetic interactions among the Co(II) ions, and no SCM behavior is observed. These results might indicate that the dimeric paddle-wheel Co(II)-carboxylate chain is essential in obtaining SCM behavior in this family of compounds. Although **2** and **7** have very similar SCM behavior, alternating current magnetic studies show that **7** has a higher energy barrier than that of **2**. Such behavior is probably caused by the larger anisotropic energy barrier in **7**.

Introduction

One of the most active topics in today's coordination chemistry is the design of molecular magnets,[1] which has the final aim of creating qubits for quantum information processing and storage. As highly expected candidates of such molecular magnets, single-molecule magnets (SMMs)[2] and single-chain magnets (SCMs)[3] have received much attention. In the past decade, many SMMs and a few of SCMs have been made. However, the blocking temperatures of up-to-date SMMs and SCMs are still too low for practical applications, and therefore the exploration of SMMs and SCMs with higher blocking temperatures (T_B) becomes an important topic for molecular magnets. As indicated by the energy barriers of SMMs ($\Delta_A = |D|S^2$ for integer spins, hereafter D refers to the zero-field splitting parameter) and SCMs ($\Delta = \Delta_A + 2\Delta_\xi = |D|S^2 + 8JS^2$), the larger sums of the D and S vectors are essential for higher T_B. However, recent theoretical studies indicate that the D and S values are extremely difficult to be simultaneously maximized, while the ideal maximum situation is one in which all the Ising-type spins are oriented parallel and ferromagnetically coupled.[4]

* To whom correspondence should be addressed. E-mail: tongml@mail.sysu.edu.cn (M.-L.T.), cxm@mail.sysu.edu.cn (X.-M.C.). Fax: (+) 86 20 8411-2245.

[†] Sun Yat-Sen University.

[‡] State University of New York at Buffalo.

(1) (a) Leuenberger, M. N.; Loss, D. *Nature* **2001**, *410*, 789. (b) Meier, F.; Levy, J.; Loss, D. *Phys. Rev. Lett.* **2003**, *90*, 047901. (c) Meier, F.; Levy, J.; Loss, D. *Phys. Rev. B* **2003**, *90*, 134417.

(2) For reviews, see (a) Christou, G.; Gatteschi, D.; Hendrickson, D. N.; Sessoli, R. *MRS Bull.* **2000**, *25*, 66–71. (b) Gatteschi, D.; Sessoli, R. *Angew. Chem., Int. Ed.* **2003**, *43*, 268–297. (c) Aromí, G.; Brechin, E. K. *Struct. Bonding (Berlin)* **2006**, *122*, 1–67.

(3) For review, see. (a) Coulon, C.; Miyasaka, H.; Clérac, R. *Struct. Bonding (Berlin)* **2006**, *122*, 163–206.

10.1021/ic801498n CCC: $40.75 © 2008 American Chemical Society
Published on Web 10/29/2008

To obtain such an ideal compound, there are probably two ways only. The first one is based on judicious ligand design. Nevertheless, the current synthetic methods of metal clusters are mostly based on self-assembly or the so-called "serendipitous assembly",[5] because "unexpected" outcomes rather than the "designed" structures can be generated. The second one is based on the modifications of known clusters; such a strategy has already been widely used in furnishing new SMMs,[6] SCMs,[7] and other higher-dimensional molecular networks with interesting magnetic properties.[8]

We recently used a σ-bonded *trans*-1,2-cyclohexanedicarboxylate (*trans*-1,2-chdc) to link anisotropic Co^{II} ions into one-dimensional (1D) chains in a two-dimensional (2D) polymer, $^{2}_{\infty}[Co^{II}$(*trans*-1,2-chdc)] (**2**), showing SCM behavior.[9] In contrast with some other Co^{II}-based SCMs,[10] the structure of **2** is somewhat unique because all the Co—O bonds are parallel and the Co^{II} ions are ferromagnetically coupled, which might fulfill the requirement of an "ideal model" with a maximized energy barrier. It is therefore, interesting to continue investigating such kind of SCMs. Usually, only very similar ligands can lead to similar structures, yet the experimental procedures may highly affect the final outcomes from the same ligand and metal ions in the same starting ratio.[9,11] Moreover, it is also meaningful to investigate the magnetic properties of other magnetically anisotropic transition metal ions like Mn^{III}, Fe^{II}, and Ni^{II} in these layered compounds,[12] since SCM behaviors are also observed in compounds with these homo- or heterospin systems. For this purpose, we extended our investigations into other magnetically anisotropic transition metal ions and *trans*-1,2-chdc analogues ligands (Scheme 1). The use of these metals and ligands leads to a new family of layered compounds that feature various metal-carboxylate chains: $^{2}_{\infty}[Fe^{II}$(*e,e-trans*-1,2-chdc)] (**3**), $^{2}_{\infty}[Ni^{II}(\mu$-$OH_2)$(*e,a-cis*-1,2-chdc)](**4**)$^{2}_{\infty}[Co^{II}(\mu$-$OH_2)$(1,2-chedc)](**5**)$^{2}_{\infty}[Co_5^{II}(\mu_3$-$OH)_2(OH_2)_2$-(1,2-chedc)$_4$] (**6**), and $^{2}_{\infty}[Co^{II}$(4-Me-1,2-chdc)] (**7**), where *cis*-1,2-chdc = *cis*-cyclohexane-1,2-dicarboxylate, 1,2-chedc = cyclohex-1-ene-1,2-dicarboxylate, and 4-Me-1,2-chdc = *trans*-4-methylcyclohexane-1,2-dicarboxylate. The syntheses, structures, and magnetic properties of these compounds will be discussed in relation with the SCM behavior observed in **2**.

Scheme 1. Structures of 1,2-chdcH_2 and Its Analogues

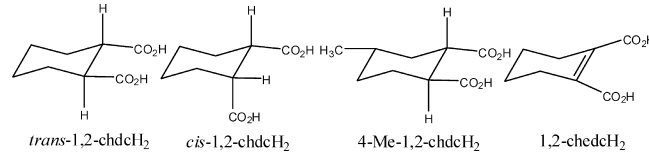

Experimental Section

Materials and Physical Measurements. Commercially available reagents were used as received without further purification. The C, H, and N microanalyses have been carried out with an Elementar Vario-EL CHNS elemental analyzer. The FT-IR spectra have been recorded from KBr pellets in the range 4000−400 cm^{-1} on a Bio-Rad FTS-7 spectrometer.

The magnetic susceptibility measurements on polycrystalline samples of **3**−**7** have been carried out on a Quantum Design MPMS-XL7 SQUID magnetometer between 1.8 and 300 K and ± 7 T. Alternating current (ac) susceptibility measurements have been performed at frequencies between 1 and 1500 Hz with an ac field of 0.0005 T and with a zero or 0.1 T applied direct current (dc) field. The zero-field cooled magnetization was obtained upon warming after zero-field cooling from 300 to 1.8 K. The field-cooled magnetization was obtained upon warming after constant 0.01 T applied field cooling from 300 to 1.8 K. Diamagnetic corrections were calculated from Pascal constants and applied to the observed magnetic susceptibility.

Typical Synthetic Procedure for $^{2}_{\infty}[Fe^{II}$(e,e-trans-1,2-chdc)] (3). A mixture of $FeSO_4 \cdot 7H_2O$ (0.278 g, 1mmol), *trans*-1,2-chdcH_2 or *cis*-1,2-chdcH_2 (0.172 g, 1 mmol), triethylamine (0.200 g, 2.0 mmol), and deioned water (10 mL) was sealed in a 23 mL Teflon-lined autoclave and heated at 160 °C for 2 days to give pale-green plate-like crystals of **3** (yield 0.15 g, 65%). IR data ($\tilde{\nu}$, cm^{-1}): 2930(m), 2845(w), 1582(vs), 1522(s), 1450(s), 1420(s), 1356(w), 1308(m), 1220(w), 1029(w), 891(w), 836(w), 767(w), 729(w), 668(w), 588(w), 522(w), 438(w). Anal. Calcd ($C_8H_{10}FeO_4$): C, 42.51; H, 4.46; Found: C, 42.80; H, 4.48%.

Typical Synthetic Procedure for $^{2}_{\infty}[Ni^{II}(\mu$-$OH_2)$(e,a-cis-1,2-chdc)] (4). A mixture of $NiCl_2 \cdot 6H_2O$ (0.238 g, 1 mmol), *cis*-1,2-chdcH_2 (0.172 g, 1 mmol), NaOH (0.200 g, 2.0 mmol) in deioned water (10 mL) was sealed in a 23 mL Teflon-lined autoclave and heated at 200 °C for 1 day to give pale-green plate-like crystals of **4** (yield

(4) (a) Waldmann, O. *Inorg. Chem.* **2007**, *46*, 10035. (b) Ruiz, E.; Cirera, J.; Cano, J.; Alvarez, S.; Loosec, C.; Kortus, J. *Chem. Commun.* **2008**, 52.
(5) Winpenny, R. E. P. *Dalton Trans.* **2002**, 1.
(6) (a) Zheng, Y.-Z.; Xue, W.; Zhang, W.-X.; Tong, M.-L.; Chen, X.-M. *Inorg. Chem.* **2007**, *46*, 6437. (b) Cornia, A.; Fabretti, A. C.; Garrisi, P.; Mortalò, C.; Bonacchi, D.; Gatteschi, D.; Sessoli, R.; Sorace, L.; Wernsdorfer, W.; Barra, A.-L. *Angew. Chem., Int. Ed.* **2004**, *43*, 1136.
(7) (a) Lecren, L.; Wernsdorfer, W.; Li, Y.-G.; Vindigni, A.; Miyasaka, H.; Clérac, R. *J. Am. Chem. Soc.* **2007**, *129*, 5045. (b) Lecren, L.; Roubeau, O.; Coulon, C.; Li, Y.-G.; Goff, X. F. L.; Wernsdorfer, W.; Miyasaka, H.; Clérac, R. *J. Am. Chem. Soc.* **2005**, *127*, 17353. (c) Toma, L. M.; Lescouëzec, R.; Pasán, J.; Ruiz-Párez, C.; Vaissermann, J.; Cano, J.; Carrasco, R.; Wernsdorfer, W.; Lloret, F.; Julve, M. *J. Am. Chem. Soc.* **2006**, *128*, 4842. (d) Bai, Y.-L.; Tao, J.; Wernsdorfer, W.; Sato, O.; Huang, R.-B.; Zheng, L.-S. *J. Am. Chem. Soc.* **2006**, *128*, 16428. (e) Xu, H.-B.; Wang, B.-W.; Pan, F.; Wang, Z.-M.; Gao, S. *Angew. Chem., Int. Ed.* **2007**, *46*, 7388. (f) Bernot, K.; Luzon, J.; Sessoli, R.; Vindigni, A.; Thion, J.; Richeter, S.; Leclercq, D.; Larionova, J.; van der Lee, A. *J. Am. Chem. Soc.* **2008**, *130*, 1619.
(8) (a) Lecren, L.; Roubeau, O.; Li, Y.-G.; Le Goff, X. F.; Miyasaka, H.; Richard, F.; Wernsdorfer, W.; Coulon, C.; Clérac, R. *Dalton Trans.* **2008**, 755. (b) Miyasaka, H.; Nakata, K.; Lollita, L.; Coulon, C.; Nakazawa, Y.; Fujisaki, T.; Sugiura, K.-i.; Yamashita, M.; Clérac, R. *J. Am. Chem. Soc.* **2006**, *128*, 3770. (c) Miyasaka, H.; Nakata, K.; Sugiura, K.-i.; Yamashita, M.; Clérac, R. *Angew. Chem., Int. Ed.* **2004**, *43*, 707.
(9) Zheng, Y.-Z.; Tong, M.-L.; Zhang, W.-X.; Chen, X.-M. *Angew. Chem., Int. Ed.* **2006**, *45*, 6310.
(10) (a) Caneschi, A.; Gatteschi, D.; Lalioti, N.; Sangregorio, C.; Sessoli, R.; Venturi, G.; Vindigni, A.; Rettori, A.; Pini, M. G.; Novak, M. A. *Angew. Chem., Int. Ed.* **2001**, *40*, 1760. (b) Liu, T.-F.; Fu, D.; Gao, S.; Zhang, Y.-Z.; Sun, H.-L.; Su, G.; Liu, Y.-J. *J. Am. Chem. Soc.* **2003**, *125*, 13976. (c) Lescouëzec, R.; Vaissermann, J.; Ruiz-Pérez, C.; Lloret, F.; Carrasco, R.; Julve, M.; Verdaguer, M.; Draomzee, Y.; Gatteschi, D.; Wernsdorfer, W. *Angew. Chem., Int. Ed.* **2003**, *42*, 1483. (d) Toma, L. M.; Lescouëzec, R.; Pasán, J.; Ruiz-Pérez, C.; Vaissermann, J.; Cano, J.; Carrasco, R.; Wernsdorfer, W.; Lloret, F.; Julve, M. *J. Am. Chem. Soc.* **2006**, *128*, 4842. (e) Sun, Z.-M.; Prosvirin, A. V.; Zhao, H.-H.; Mao, J.-G.; Dunbar, K. R. *J. Appl. Phys.* **2005**, *97*, 10B305/1. (f) Li, X.-J.; Wang, X.-Y.; Gao, S.; Cao, R. *Inorg. Chem.* **2006**, *45*, 1508.
(11) Zheng, Y.-Z.; Tong, M.-L.; Zhang, W.-X.; Chen, X.-M. *Chem. Commun.* **2006**, 165.
(12) Zheng, Y.-Z.; Xue, W.; Tong, M.-L.; Chen, X.-M.; Grandjean, F.; Long, G. J. *Inorg. Chem.* **2008**, *47*, 4077.

Table 1. Data Collection and Structural Refinement Parameters for **3**−**7**

	3	**4**	**5**	**6**	**7**
formula	$C_8H_{10}FeO_4$	$C_8H_{12}NiO_5$	$C_8H_{10}CoO_5$	$C_{32}H_{28}Co_5O_{20}$	$C_9H_{12}CoO_4$
f.w.	226.01	246.87	245.09	1037.28	243.12
T (K)	298(2)	293(2)	288(2)	293(2)	293(2)
space group	$P\bar{1}$ (No. 2)	$C2/c$ (No. 15)	$C2/c$ (No. 15)	$P\bar{1}$ (No. 2)	$P\bar{1}$ (No. 2)
a (Å)	5.2211(6)	25.881(7)	27.083(2)	7.2231(4)	5.1304(4)
b (Å)	6.5621(8)	6.858(4)	6.7649(6)	9.1683(6)	6.5104(6)
c (Å)	13.360(2)	10.376(6)	9.4850(8)	14.5105(9)	14.984(1)
α (deg)	99.450(2)	90	90	74.563(1)	88.659(1)
β (deg)	98.571(2)	98.96(2)	95.844(2)	78.838(1)	81.184(1)
γ (deg)	102.775(2)	90	90	82.749(1)	78.020(1)
V (Å^3)	432.10(9)	1819.2(16)	1728.7(3)	905.9(1)	483.76(7)
Z	2	8	8	2	2
D_c (g cm^{-3})	1.737	1.803	1.883	1.901	1.669
μ (mm^{-1})	1.721	2.125	1.976	2.328	1.757
data collected/unique	3151/1664	6252/1734	4280/1661	7039/3511	3633/1849
R_1 (>2σ/all data)	0.0316/0.0343	0.0664/0.0885	0.0308/0.0375	0.0344/0.0374	0.0509/0.0587
wR_2 (>2σ/all data)	0.0750/0.0766	0.1481/0.1591	0. 0743/0. 0769	0.0937/0.0959	0.1257/0.1298
GOF	1.071	1.027	1.037	1.026	1.074
residues (e Å^{-3})	–0.272/0.508	–0.857/3.171	–0.308/0.389	–0.578/1.145	–0.583/1.437

0.092 g, 37%), IR data ($\tilde{\nu}$, cm^{-1}): 2958(m), 1603(vs), 1539(s), 1445(s), 1415(s), 1332(m), 1293(w), 1236(w), 1115(w), 1033(w), 933(w), 860(w), 775(w), 708(m), 615(w), 526(w), 445(w). Anal. Calcd ($C_8H_{12}NiO_5$): C, 38.92; H, 4.90; Found: C, 38.88; H, 4.98%.

Typical Synthetic Procedure for $^2_\infty$[Co^{II}(μ-OH$_2$)(1,2-chedc)] (5). A mixture of $CoCl_2 \cdot 6H_2O$ (0.237 g, 1 mmol), 3,4,5,6-tetrahydrophthalic anhydride (0.168 g, 1 mmol) and triethylamine (0.200 g, 2 mmol) in deioned water (10 mL) was sealed in a 23 mL Teflon-lined autoclave and heated at 170 °C for 3 days to give pink needle-like crystals of **4** (yield 0.14 g, 57%), IR data ($\tilde{\nu}$, cm^{-1}): 3425(s), 2931(m), 1550(vs), 1375(s), 1328(s), 988(w), 880(w), 729(w), 450(w). Anal. Calcd ($C_8H_{10}CoO_5$): C, 39.20; H, 4.11; Found: C, 39.22; H, 4.13%.

Typical Synthetic Procedure for $^2_\infty$[Co$_5^{II}$(μ_3-OH)$_2$(OH$_2$)$_2$(1,2-chedc)$_4$] (6). It was synthesized as for **5** by using KOH (0.112 g, 2 mmol) in place of triethylamine. Purple plate-like crystals of **6** were isolated in 5% yield (0.011 g), IR data ($\tilde{\nu}$, cm^{-1}): 3424(m), 2931(s), 2857(w), 1547(vs), 1418(s), 1384(s), 1333(s), 1070(w), 968(w), 833(w), 805(w), 784(w), 734(w), 638(w), 446(w). Anal. Calcd ($C_{32}H_{28}Co_5O_{20}$): C, 37.42; H, 2.75; Found: C, 37.38; H, 2.78%.

Typical Synthetic Procedure for $^2_\infty$[Co^{II}(4-Me-1,2-chdc)] (7). A mixture of $CoCl_2 \cdot 6H_2O$ (0.237 g, 1 mmol), hexahydro-4-methylphthalic anhydride (*cis*- and *trans*- mixture) (0.186 g, 1 mmol) and 1,4-diazabicyclo[2,2,2]octane (0.056 g, 0.5 mmol) in deioned water (10 mL) was sealed in a 23 mL Teflon-lined autoclave and heated at 170 °C for 3 days to give dark-red plate-like crystals of **7** (yield 0.22 g, 89%), IR data ($\tilde{\nu}$, cm^{-1}): 2959(m), 2925(m), 1605(vs), 1543(s), 1449(s), 1418(s), 1337(m), 1295(w), 1239(w), 1118(w), 1035(w), 935(w), 861(w), 776(w), 710(m), 617(w), 528(w), 449(w). Anal. Calcd ($C_9H_{12}CoO_4$): C, 44.46; H, 4.97; Found: C, 44.42; H, 4.98%.

X-ray Crystallography. Single-crystal X-ray diffraction intensities of **3**−**7** have been collected on a Bruker Apex CCD area-detector diffractometer by using MoKα ($\lambda = 0.71073$ Å) radiation. Absorption corrections have been applied by using the multiscan program SADABS.[13] The structures were solved with direct methods and refined with a full-matrix least-squares technique with the SHELXTL program package.[14] Anisotropic thermal parameters have been assigned to all non-hydrogen atoms. The organic hydrogen atoms were generated geometrically. Data collection and structural refinement parameters are given in Table 1, and selected bond distances and angles are given in Table 2.

Results and Discussion

Syntheses. It is noteworthy that the conformations of cyclohexane-1,2-dicarboxylate (1,2-chdc) observed in these series of compounds are interesting. As shown in our previous Density-Functional-Theory (DFT) studies,[15] the energy barrier of the *trans* conformation of 1,2-chdc is only about 90 kJ mol^{-1} higher than that of the *cis* conformation, and therefore, the conformations of 1,2-chdc can be significantly affected by the synthetic conditions such as solvents, temperature, pressure, and the cooperative effect of coordination with the metal ions. Thus, the final conformations of 1,2-chdc can not be predicted well. For example, we isolated a Mn^{II} compound of *cis*-1,2-chdc by using ethylene glycol as the solvent, while the *trans* conformation compound was obtained if water was used instead.[15] Moreover, no matter which solvent was used and how long the reaction time was, the *trans* products were always obtained in the presence of Co^{II} and Fe^{II} ions. In this work, we used shorter reaction time to obtain the *cis* products in the presence of Ni^{II} ions, but we were unable to obtain other well crystallized products no matter how we prolonged the reaction time. To rationalize the presence of the *cis* or *trans* form of 1,2-chdc requires more experimental and theoretical study.

Nevertheless, this synthetic method can be applied to the structurally related 1,2-chedcH$_2$ and 4-Me-1,2-chdcH$_2$ ligands to obtain compounds with linear metal−oxygen chains. By using 1,2-chedcH$_2$, we isolated two new compounds, namely aqua-bridged $^2_\infty$[Co^{II}(μ-OH$_2$)(1,2-chedc)] (**5**) and hydroxyl-bridged $^2_\infty$[Co$_5^{II}$(μ_3-OH)$_2$(OH$_2$)$_2$(1,2-chedc)$_4$] (**6**) at lower and higher pH condition, respectively. In contrast, the metal−oxygen chains in these two compounds are different from those of **2**. We believe that the structural change can be attributed to the rigid C═C bond between two carboxylates in 1,2-chedc rather than the flexible C—C bond in 1,2-chdc. If the flexible 4-Me-1,2-chdcH$_2$ was employed, we were then able to obtain

(13) Sheldrick, G. M. *SADABS 2.05*; University Göttingen: Göttingen, Germany, 2002.

(14) *SHELXTL 6.10*; Bruker Analytical Instrumentation: Madison, WI, 2000.

(15) Zheng, Y.-Z.; Xue, W.; Zheng, S.-L.; Tong, M.-L.; Chen, X.-M. *Adv. Mater.* **2008**, *20*, 1534.

Table 2. Selected Bond Lengths (Å) and Bond Angles (deg) for **2**−**7**

				2[a]			
Co1−O1	1.971(3)	Co1−O2$^{a\#}$	1.986(3)	Co1−O4$^{b\#}$	2.019(3)	Co1−O3$^{c\#}$	2.044(3)
Co1−O4$^{d\#}$	2.210(3)	Co1···Co1$^{a\#}$	2.912(1)	Co1···Co1$^{f\#}$	3.269(1)	Co1$^{b\#}$−O4−Co1$^{e\#}$	101.1(1)
				3[b]			
Fe1−O1	2.229(2)	Fe1−O2$^{d\#}$	2.079(2)	Fe1−O4$^{b\#}$	2.013(2)	Fe1−O1$^{c\#}$	2.072(2)
Fe1−O3$^{a\#}$	1.997(2)	Fe1···Fe1$^{d\#}$	2.8419(7)	Fe1···Fe1$^{f\#}$	3.3939(7)	Fe1$^{c\#}$−O1−Fe1	104.13(7)
				4[c]			
Ni1−O3$^{a\#}$	1.985(4)	Ni1−O1	2.025(4)	Ni1−O4$^{c\#}$	2.023(4)	Ni1−O1w	2.210(3)
Ni1−O2$^{b\#}$	1.991(4)	Ni1−O1w$^{b\#}$	2.033(4)	Ni1···Ni1$^{d\#}$	3.457(2)	Ni1$^{d\#}$−O1w−Ni1	109.1(2)
				5[d]			
Co1−O1	2.009(2)	Co1−O4$^{b\#}$	2.079(2)	Co1−O1w	2.214(2)	Co2−O4$^{c\#}$	2.127(2)
Co2−O3$^{b\#}$	2.068(2)	Co2−O1w	2.101(2)	Co1···Co2	3.146(2)	Co1−O1w−Co2	93.59(7)
Co1$^{g\#}$−O4−Co2$^{g\#}$	96.81(7)						
				6[e]			
Co1−O8$^{a\#}$	2.016(2)	Co1−O5	2.173(2)	Co1−O9	2.084(2)	Co2−O7$^{a\#}$	2.028(2)
Co2−O2	2.290(2)	Co2−O9	2.063(2)	Co2−O5	2.162(2)	Co3−O9	1.947(2)
Co2−O1w	2.084(2)	Co2−O4$^{d\#}$	2.099(2)	Co3−O1	1.944(2)	Co3−O3$^{b\#}$	1.990(2)
Co3−O6$^{c\#}$	1.944(2)	Co1···Co2	3.094(2)	Co1···Co3	3.273(2)	Co2···Co3	3.423(2)
Co2−O5−Co1	91.08(7)	Co3−O9−Co2	117.2(1)	Co2−O9−Co1	96.50(8)	Co3−O9−Co1	108.53(9)
				7[f]			
Co1)−O1	1.962(3)	Co1−O2$^{a\#}$	1.981(3)	Co1−O4$^{b\#}$	2.013(2)	Co1−O3$^{c\#}$	2.031(3)
Co1)−O4$^{d\#}$	2.206(3)	Co1···Co1$^{a\#}$	2.8974(9)	Co1···Co1$^{f\#}$	3.253(1)	Co1$^{b\#}$−O4−Co1$^{e\#}$	100.8(1)

[a] Symmetry codes for **2**: (a#) $-x+2, -y+1, -z+1$; (b#) $-x+1, -y+2, -z+1$; (c#) $-x+2, -y+2, -z+1$; (d#) $x, y-1, z$; (e#) $x, y+1, z$; (f#) $-x+1, -y+1, -z+1$. [b] Symmetry codes for**3**: (a#) $x, y+1, z$; (b#) $-x, -y-1, -z$; (c#) $-x+1, -y, -z$; (d#) $-x, -y, -z$. [c] Symmetry codes for **4**: (a#) $x, -y+1, z-1/2$; (b#) $-x+1/2, y+1/2, -z+1/2$; (c#) $-x+1/2, -y+1/2, -z+1$; (d#) $-x+1/2, y-1/2, -z+1/2$. [d] Symmetry codes for **5**: (b#) $-x+1, y-1, -z+1/2$; (c#) $x, y-1, z$; (g#) $x, y+1, z$. [e] Symmetry codes for **6**: (a#) $-x, -y+1, -z+2$; (b#) $x+1, y, z$; (c#) $-x+1, -y+1, -z+2$; (d#) $-x, -y+2, -z+2$. [f] Symmetry codes for **7**: (a#) $-x+2, -y+1, -z+1$; (b#) $-x+1, -y+2, -z+1$; (c#) $-x+2, -y+2, -z+1$; (d#) $x, y-1, z$; (e#) $x, y+1, z$; (f#) $-x+1, -y+1, -z+1$.

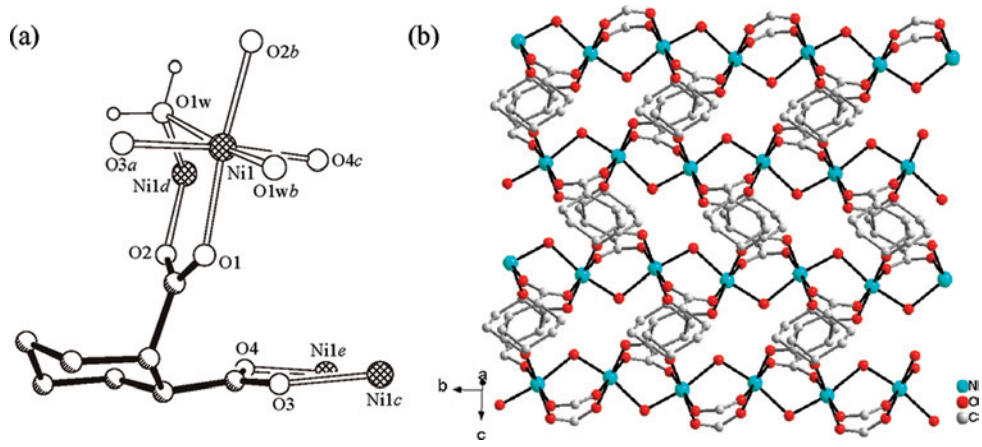

Figure 1. Coordination environment (a) (symmetry codes: [a] $x, -y+1, z-1/2$; [b] $-x+1/2, y+1/2, -z+1/2$; [c] $-x+1/2, -y+1/2, -z+1$; [d] $-x+1/2, y-1/2, -z+1/2$; [e] $x, 1-y, z+1/2$) and the layered structure (b) in **4**.

$^{2}_{\infty}$[Co^{II}(4-Me-1,2-chdc)] (**7**), which is isomorphous to **2**. These results show that the flexible C—C bond and the *trans* configuration between two carboxylates are critical to maintain the framework structure of **2**.

Structural Characterization. The crystal structure of **3** is isomorphous with **2**, as shown in Supporting Information, Figure S1. The Fe—O chain is also constructed by the tetracarboxylate-bridged paddle-wheel Fe^{II} dimers. The intradimer Fe^{II}···Fe^{II} distance is 2.842 Å, being slightly shorter than that in **2**. However, the interdimer Fe^{II}···Fe^{II} distance and Fe—O—Fe angle of bis(μ-η^2)-carboxylate-bridged Fe^{II} ions is 3.393(1) Å and 104.1(1)°, respectively. These values are slightly larger than those in **2**, as shown in Table 2. Such Fe—O chains are further connected by the *trans*-1,2-chdc into 2D layers, which are also stacked only by van der Waals interactions with the shortest interlayer Fe^{II}···Fe^{II} distance of 12.0 Å.

As shown in Figure 1a, each asymmetric unit contains one Ni^{II} ion, one μ-aqua molecule, and one *e*,*a*-*cis*-1,2-chdc ligand. The octahedral Ni^{II} ions are bridged by *trans*-related axial aqua (Ni—O$_{aqua}$—Ni 109.1(2)°) and two syn-syn-μ-η^1:η^1 carboxylate ligands. As shown in Figure 1b, the Ni—O chain goes along the *b*-axis with equal Ni^{II}···Ni^{II} distances of 3.457 Å. However, the Ni^{II} ion does not sit on an inversion center but a 2_1-screw axis running along the *b*-axis. The function of *e*,*a*-*cis*-1,2-chdc is similar to those in **2** and **3**, which connects the Ni—O chains to form a 2D layer with a shortest interchain Ni^{II}···Ni^{II} distance of 5.539 Å. The layers are also stacked only via van der Waals interactions with the shortest Ni^{II}···Ni^{II}distance up to 12.92 Å.

As shown in Figure 2, the asymmetric unit of **5** contains two half-occupied Co^{II} ions, one μ-aqua molecule, and one 1,2-chedc ligand. It is interesting that Co1 and Co2 have elongated and compressed octahedral geometries, respec-

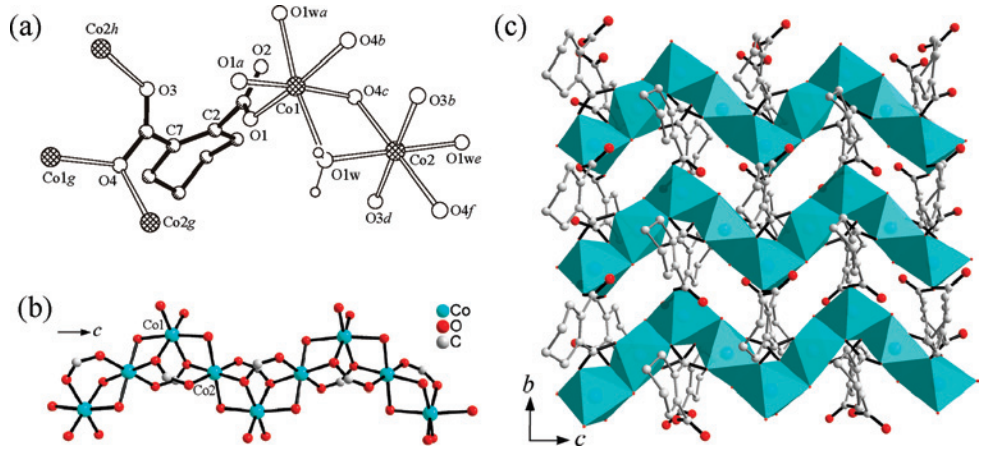

Figure 2. Coordination environments (a), Co—O chain (b) and layer (c) in **5**. Symmetry codes: [a] $-x+1, y, -z+1/2$; [b] $-x+1, y-1, -z+1/2$; [c] $x, y-1, z$; [d] $x, -y+2, z+1/2$; [e] $-x+1, -y+1, -z+1$; [f] $-x+1, -y+2, -z+1$; [g] $x, y+1, z$; [h] $-x+1, y+1, -z+1/2$.

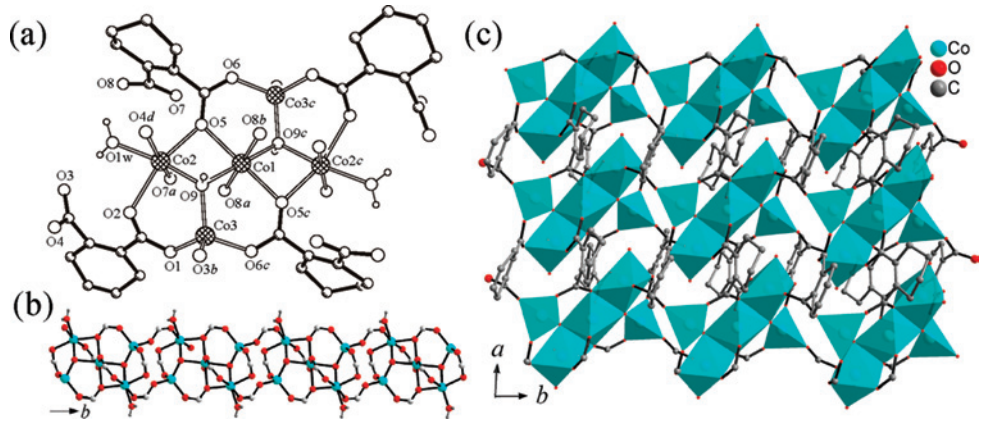

Figure 3. Coordination environments (a), Co—O chain (b), and *ab*-plane layered structure (c) in **6**. Symmetry codes: [a] $-x, -y+1, -z+2$; [b] $x+1, y, z$; [c] $-x+1, -y+1, -z+2$; [d] $-x, -y+2, -z+2$.

tively. The elongated axial positions of Co1 are occupied by two aqua molecules (Co—O 2.214(2) Å) while the equatorial plane is coordinated by four carboxylate oxygen atoms (Co—O 2.009(2)−2.079(2) Å). The compressed axial positions of Co2 are coordinated by two carboxylate oxygen atoms (Co—O 2.068(2) Å) and the equatorial plane is coordinated by a pair of *trans*-related carboxylate oxygen atoms and a pair of *trans*-related aqua molecules (Co—O 2.101(2)−2.127(2) Å). Being different with **4**, the zigzag Co—O chain goes along the *c* direction rather than the *b* direction. It should be noted that the equatorial planes of the intrachain adjacent to Co2 ions have a dihedral angle of 47.2°. The Co—O chain consists of edge-sharing octahedral Co^{II} ions with equal space ($Co^{II}\cdots Co^{II}$ 3.146(2) Å). The bridging oxygen atoms are from one μ_3-carboxylate end (O4) and one μ-aqua ligand (O1w). The shortest $Co^{II}\cdots Co^{II}$ distance between adjacent chains is 5.262 Å, and the layers are stacked throught van der Waals interaction with the shortest $Co^{II}\cdots Co^{II}$ distance up to 13.57 Å.

As shown in Figure 3, the asymmetric unit of **6** contains two and a half Co^{II} ions, one μ_3-hydroxide, one terminal aqua, and two 1,2-chedc ligands. The Co1 ion sits on the inversion center in an elongated octahedral geometry, in which the axial positions are occupied by two carboxylate oxygen atoms (Co—O 2.173(2) Å), and the equatorial positions are occupied by two other carboxylate oxygen (Co—O 2.016(2) Å) and two hydroxide oxygen atoms (Co—O 2.084(2) Å). The μ_3-OH group further connects with two other Co^{II} ions, octahedral Co2, and tetrahedral Co3. Co2 is coordinated by six oxygen atoms from one aqua (Co—O 2.084(2) Å), one hydroxide (Co—O 2.063(2) Å), and four carboxylates (Co—O 2.028(2)−2.290(2) Å). Co3 is coordinated by four oxygen atoms from one hydroxide (Co—O 1.947(2) Å) and three carboxylates (Co—O 1.944(2)−1.990(2) Å). Thus, a pentanuclear $[Co_5(\mu_3\text{-}OH)_2]^{8+}$ unit forms, which consists of three edge-sharing octahedral Co^{II} ions in the "body" with two corner-sharing tetrahedral Co^{II} ions at both sides. The pentanuclear units are connected by the syn-anti carboxylates into the chains along the *b*-axis ($Co^{II}\cdots Co^{II}$ 5.500 Å), which are connected by 1,2-chedc into a layer with the shortest $Co^{II}\cdots Co^{II}$ distance of 5.034 Å. Such layers are further stacked by van der Waals interactions with the shortest $Co^{II}\cdots Co^{II}$ distance up to 10.25 Å.

Compound **7** is structurally very similar to that of **2** (Figure 4),[9] which also features Co^{II}-carboxylate chains based on paddle-wheel dimers, being further linked by 4-Me-1,2-chdc into 2D layers. These layers are also stacked only by van der Waals interactions with the shortest $Co^{II}\cdots Co^{II}$ distance up to 13.71 Å, which is significantly larger than 12.08 Å in **2** because of the presence of a methyl group. More importantly, all the Co—O bonds, $Co^{II}\cdots Co^{II}$ distances, and Co—O—Co angle in **7** are slightly shorter or smaller than

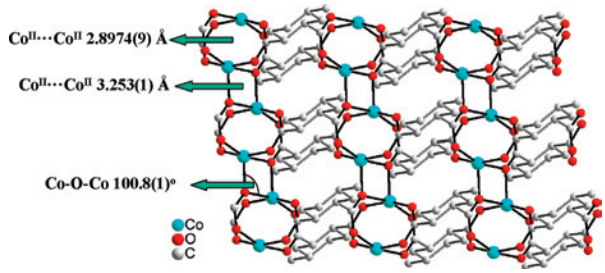

Figure 4. Perspective view of the layer in **7**.

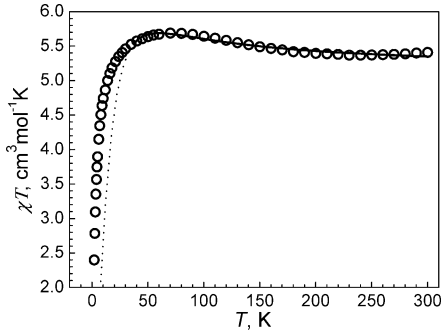

Figure 5. Plot of χT vs T at an applied field of 500 Oe from 2 to 300 K in **3**. Solid line: the fitting curve with the Fisher model from 300 to 35 K. Dotted line: the extrapolation of the fitting curve from 30 to 2 K.

the corresponding ones in **2** (Table 2). These small changes of Co—O bonds and Co—O—Co angles have not led to a marked change of the structure but have perturbations on the magnetic properties of this structure (vide infra).

Non-SCM Behaviors in 3−6. As shown in Figure 5, the χT value of **3** at room temperature is 5.41 cm^3 mol^{-1} K, significantly large than the spin-only value of Fe^{II} (3.00 cm^3 mol^{-1} K), indicating a large spin−orbital contribution of the Fe^{II} ion in the square-pyramidal geometry. Upon cooling, the χT slightly decreases to a minimum of 5.37 cm^3 mol^{-1} K at 240 K and then gradually increases, reaching a maximum of 5.69 cm^3 mol^{-1} K at 70 K. This shape of the χT plot is usually indicative of uncompensated spins similar to those in ferrimagnets, weak ferromagnets, alternating antiferromagnetic-ferromagnetic (AF-F) spin chains, and/or compounds containing orbitally degenerate magnetic ions, such as Fe^{II} ions herein. The large decrease of the χT plot below 30 K is expected for zero-field splitting of Fe^{II} ions or significant interchain AF interaction. To study the magnetic interactions in **3**, a Heisenberg−Fisher model (eq 1) was used to fit the data above 30 K,[17]

$$\hat{H} = -J_1 \sum_{i=1}^{N} S_{2i} S_{2i+1} - J_2 \sum_{i=1}^{N} S_{2i} S_{2i+2} \qquad (1)$$

where J_1 and J_2 are magnetic interactions in the chain (note that this model can be reduced to the uniform chain if $J_1 = J_2$). The best fitting gives $J_1/k_B = 9.7(5)$ K, $J_2/k_B = -3.7(1)$ K, and $g = 2.623(5)$. The opposite signs of J indicate the alternating F-AF exchange coupling interactions in the chain. The larger magnitude of the positive J_1 suggests a stronger

(16) (a) Kahn, O. *Molecular Magnetism*; VCH: New York, 1993. (b) Carlin, R. L. *Magnetochemistry*; Springer: Berlin, 1986.
(17) Fisher, M. E. *Am. J. Phys* **1964**, *32*, 343.

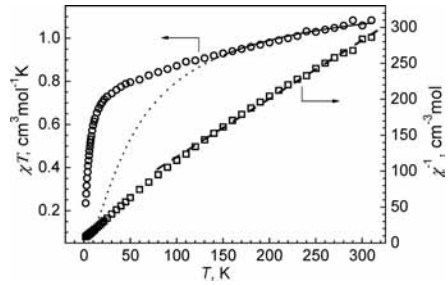

Figure 6. Left: plot of χT vs T at an applied field of 500 Oe from 2 to 310 K in **4**. Solid line: the fitting curve with the Fisher model from 310 to 150 K. Dotted line: the extrapolation of the fitting curve from 150 to 2 K. Right: the temperature-dependent inverse susceptibility of **4**. Dashed line: the fitting curve of the Curie−Weiss law.

ferromagnetic interaction within the chain, which could probably be due to the bis(μ^2-η^2)-carboxylate bridge between the Fe^{II} ions. However, we can not exclude the possiblity of ferromagnetic interaction through the 4-fold syn-syn carboxylate bridge. The data below 30 K can not be fitted by this Heisenberg model, which indicates that a more complicated Hamiltonian including single-ion magnetic anisotropy and spin−orbital coupling is necessary. As indicated in the ac susceptibility data (Supporting Information, Figure S2), such intrachain F-AF interaction does not lead to either an SCM or a long-range magnetic ordering behavor in **3** since no slow-relaxation or sharp peaks were observed. In addition, the unsaturated $M(H)$ plot even up to 7 T at 2 K confirms the magnetic behavior of anisotropic iron(II) ions.

The dc susceptibility data of **4** (Figure 6) show a χT value of 1.08 cm^3 mol^{-1} K at room temperature, which is very close to that expected for a spin-only Ni^{II} ion (1.00 cm^3 mol^{-1} K). Upon cooling, χT continuously decreases. The inverse molecular magnetic susceptibility, χ^{-1}, obeys the Curie−Weiss law from 100−310 K and can be fitted with Curie−Weiss constants, C and θ, of 1.23 cm^3 mol^{-1} K and −47.5 K, respectively. The C value corresponds to an effective magnetic moment of 3.14 μ_B, and the large negative θ value indicates significant AF interactions between the Ni^{II} ions. A 1D Fisher chain model (for $S = 1$),[17] $\hat{H} = -J\sum S_i S_{i+1}$, was tried to fit the data. However, this Heisenberg model can not fit the data well below 150 K, as shown in Figure 6. The dotted line represents the extrapolation of curve above 150 K with parameters of $J/k_B = -23(1)$ K and $g = 2.22(1)$. The failure of this model may indicate that the effect of zero-field splitting and/or interchain interactions can not be neglected at low temperature. Similar to that of **3**, **4** does not show either SCM or long-range magnetic ordering behavior. The χT plot decreases quickly below 30 K, which may also indicate large zero-field splitting effect of the Ni^{II} ions or interchain AF interaction, leading to a diamagnetic ground state. As shown in the Supporting Information, Figure S3, the ac susceptibility data of **4** also show only a paramagnetic-like behavior down to 2 K. In addition, the 2 K $M(H)$ plot increases almost linearly and does not show saturation up to 7 T, which is probably consistent with the observed intrachain AF interactions in **4**.

The dc susceptibility data (Figure 7) measured on a powder sample of **5** show that the χT value of **5** at 320 K is 3.20 cm^3 mol^{-1} K per Co^{II}, being significantly larger than the spin-

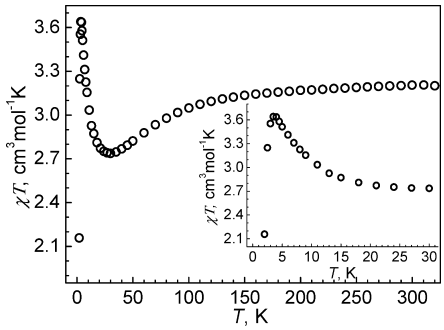

Figure 7. Plot of χT vs T at an applied field 500 Oe from 2 to 320 K in **5**. Inset: enlarged χT vs T plot from 2−30 K.

Scheme 2. Spin-Coupling Scheme of the Δ-Chain in **5**

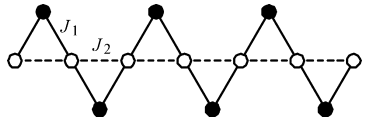

Scheme 3. Spin-Chain Coupling Scheme of **6**

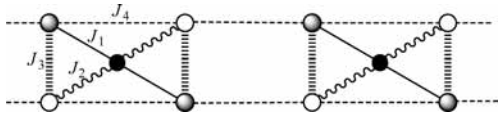

only value of 1.88 cm^3 mol^{-1} K and hence also indicates large orbital contribution.[16] Upon cooling, it gradually decreases to about 30 K with the presence of a minimum of 2.74 cm^3 mol^{-1} K, and then it increases to a maximum of 3.64 cm^3 mol^{-1} K at 3.5 K. The data in the range of 40−320 K obeys the Curie−Weiss law with $C = 3.29$ cm^3 mol^{-1} K and $\theta = -7.87$ K. From the chain structure of **5** (Figure 2b), one can get that the main magnetic exchange coupling ways are a typical corner-sharing triangular chain, or called Δ-chain, which is part of a Kagomé lattice,[18] as shown in Scheme 2. There are two main magnetic exchange coupling ways. J_1 is via the (μ-aqua)(μ-carboxylate)-bridge, and J_2 is through the syn-anti μ-carboxylate-bridge between the Co^{II} ions. However, the f value, which can be used to measure the extent of spin-frustration, is defined as $f = |\theta/T_c|$. For **5**, $f = |7.87/3.5| = 2.24 < 5$ does not suggest any spin-frustration effect.[19] Magnetic competitions such as ferro- and/or antiferromagnetic interactions are responsible for the non-diamagnetic ground-state in **5**.[20] The $M(H)$ plot gives the maximum value of 2.40 μ_B at 7 T, which is consistent with a typical value of one uncompensated octahedral Co^{II} ion (Supporting Information, Figure S4).[16,21,22]

Compound **6** has a pentanuclear Co^{II}-based spin-chain, as shown in Scheme 3. The dc susceptibility data (Figure 8) measured on a powder sample of **6** show that the χT value of **6** at 320 K is 16.90 cm^3 mol^{-1} K per $Co^{II}{}_5$, which is significantly larger than the spin-only value of 9.38 cm^3 mol^{-1} K, hence indicating a large orbital contribution. Upon cooling, χT continuously decreases to 2.0 K. The data in the range of 20−320 K obeys the Curie−Weiss law with $C = 19.96$ cm^3 mol^{-1} K and $\theta = -62.37$ K. This large negative θ value indicates not only spin−orbital coupling of the Co^{II} ion but also significant AF interactions between the Co^{II} ions, which are caused by the more effective magnetic communication via the μ_3-OH groups. The θ value is consistent with those of reported Co^{II} compounds with μ_3-OH bridges.[11] The ac susceptibility data (inset of Supporting Information, Figure S5) also do not suggest any slow-relaxation behavior in **6**. In addition, the maximum value of the $M(H)$ plot is 3.81 μ_B at 7 T (Supporting Information, Figure S5), being significantly below the expected value for a $Co^{II}{}_5$ unit, which is consistent with the AF interactions between the spins.

SCM Behavior in 7. The dc susceptibility data (Figure 9) measured on a powder sample of **7** show that the χT value at room temperature is 3.32 cm^3 mol^{-1} K per Co^{II}, which is much larger than the spin-only value (1.88 cm^3 mol^{-1} K), as well as that (2.98 cm^3 mol^{-1} K) of **2**, hence indicating a very large orbital contribution even larger than that of **2**. Upon cooling, it gradually decreases to a minimum of 3.28 cm^3 mol^{-1} K at 176 K, and then increases. When fitting χ^{-1} vs T data from 304 to 176 K with the Curie−Weiss law, one gets $C = 3.39$ cm^3 mol^{-1} K and $\theta = -6.73$ K (Supporting Information, Figure S6).

Below 30 K, the χT value increases quickly up to a maximum value of 62.84 cm^3 mol^{-1} K at 5.8 K. Because the square-pyramidal Co^{II} ions have the similar effective spin-1/2 as that of the octahedral Co^{II} ions because of the combined action of spin−orbital coupling and noncubic

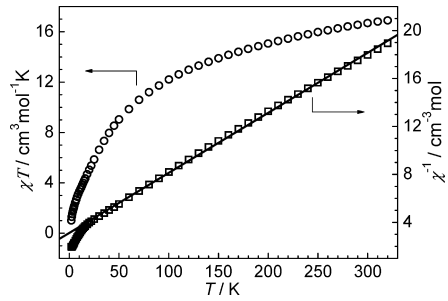

Figure 8. Left: plot of χT vs T at an applied field of 500 Oe from 2 to 320 K in **6**. Right: the temperature-dependent inverse susceptibility of **6**. Solid line: the fitting curve with the Curie−Weiss law.

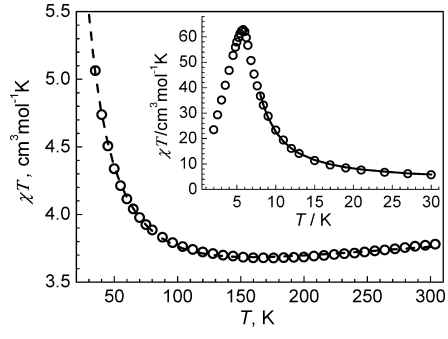

Figure 9. Plot of χT vs T at an applied field of 1 KOe from 35 to 304 K in **7**. Dashed line: fitted by eq 5. Inset: χT vs T plot from 2−30 K. Solid line: fitted by spin-1/2 alternating Ising chain model.

(18) (a) Zheng, Y.-Z.; Xue, W.; Tong, M.-L.; Chen, X.-M.; Grandjean, F.; Long, G. J. *Angew. Chem., Int. Ed.* **2007**, *46*, 6076. (b) Cheng, X.-N.; Zhang, W.-X.; Zheng, Y.-Z.; Chen, X.-M. *Chem. Commun.* **2006**, 3603. (c) Cave, D.; Coomer, F. C.; Molinos, E.; Klauss, H.-H.; Wood, P. T. *Angew. Chem., Int. Ed.* **2006**, *45*, 803.

(19) (a) Ramirez, A. P. *Annu. Rev. Mater. Sci.* **1994**, *24*, 453. (b) Greedan, J. E. *J. Mater. Chem.* **2001**, *11*, 37. (c) Harrison, A. *J. Phys.: Condens. Matter* **2004**, *16*, S553.

(20) Chikazumi, S. *Physics of Ferromagnetism*; Clarendon Press, Oxford Science Publications: Oxford, 1997.

crystal-field terms, giving six-Kramers doublets at low temperatures,[16,22] the data below 30 K can be treated as a spin-1/2 Ising chain with alternating space sites, namely, with two nearest neighbor interactions (J and j), and alternating Landé factors (g_a and g_b). The full Hamiltonian is written as follows[23]

$$\hat{H} = -J\sum_{i=1}^{N} S^z_{2i-1}S^z_{2i} - j\sum_{i=1}^{N} S^z_{2i}S^z_{2i+1} - \left(g_a\sum_{i=1}^{N} S^z_{2i-1} + g_b\sum_{i=1}^{N} S^z_{2i}\right)\mu_B H \quad (2)$$

where S^z_i stands for the z component of the spin operator located on site i, μ_B is the Bohr magneton, and H is the external magnetic field. This Hamiltonian was solved by using the transfer matrix method by Drillon et al.,[23,24] giving rise into the final analytical expressions, or eqs 3 and 4.

$$\chi_{\parallel} = \frac{N\mu_B^2}{2k_BT}\frac{g_+^2\exp(J_+/2k_BT) + g_-^2\exp(J_-/2k_BT)}{\cosh(J_-/2k_BT)} \quad (3)$$

$$\chi_{\perp} = \frac{Ng_{\perp}^2\mu_B^2}{2J}[\tanh(J/4k_BT) + (J/4k_BT)\,\mathrm{sech}^2(J/4k_BT)] \quad (4)$$

where $g_{\pm} = (g_a \pm g_b)/2$ and $J_{\pm} = (J \pm j)/2$. In the case of **7**, the alternating Landé factors (g_a and g_b) can be simplified to $g_a = g_b = g$ because all the Co^{II} ions are crystallographically identical. For a powder sample of **7**, $\chi_m = {}^1/_3\chi_{\parallel} + {}^2/_3\chi_{\perp}$ was applied to obtain an average value. During the fitting process, we found that $g_{\perp}$ tends to be zero, and the best fit (from 30 to 9 K) gives $g_{\parallel} = 6.6(1)$, $g_{\perp} = 0$, $J = 36(5)$ cm^{-1}, and $j = 25(1)$ cm^{-1} (see the inset of Figure 9). The large value of $g_{\parallel}$ indicates strong magnetic anisotropy of the Co^{II} ions, which is consistent with other reported Co^{II} ions with octahedral, square-pyramidal, or triangular-bipyramidal geometries.[16,22,23] The unequal, large positive coupling constants indicate strong alternating ferromagnetic interactions in **7**, which is consistent with those of **2**. For comparison, the same equations were applied to fit the χT data of **2** from 30 to 9 K, giving the best fitting parameters of $g_{\parallel} = 5.7(4)$, $g_{\perp} = 0$, $J = 57(12)$ cm^{-1}, and $j = 26.2(8)$ cm^{-1}, as shown in Supporting Information, Figure S7. These values show that the ferromagnetic interactions in **2** are stronger than those in **7**, while the $g_{\parallel}$ value of **2** is slightly smaller than that of **7**. The larger $g_{\parallel}$ value of **7** may suggest that the spin−orbital coupling effect in **7** is enhanced in comparison to that of **2**. This conclusion is consistent with the observed decrease of χT vs T plot of **7** at higher temperatures. The well-fitted curve confirms that the magnetic behavior of **7** is indeed consistent with the Ising model rather than a 3D long-range magnetic ordering behavior.

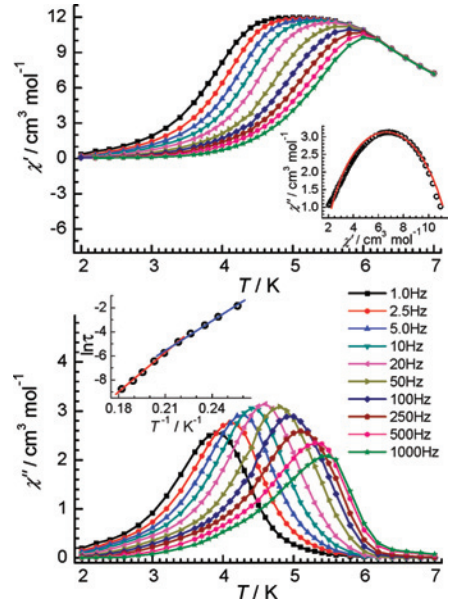

Figure 10. Top: real part of ac susceptibility, inset: Cole−Cole diagram at 4.2 K. Bottom: imaginary part of ac susceptibility; inset: the peak temperatures of χ'' fitted by the Arrhenius law for **7**.

To better understand the ground-state of **7**, the χT data were fitted by eq 5,[25]

$$\chi T = C_1\exp(\alpha J/k_BT) + C_2\exp(\beta J/k_BT) \quad (5)$$

where $\alpha J < 0$ indicates the spin−orbital coupling of the Co^{II} ions, being responsible for the initial high temperature decay of χT; $\beta J > 0$ denotes the ferromagnetic-like interaction, leading to the increase of χT at low temperatures. C_1+C_2 equals the Curie constant at high temperatures. Fitting the data from 304 to 35 K (Figure 9) gives $\alpha J/k_B = -265(11)$ K, $C_1 = 0.77(1)$ cm^3 mol^{-1} K, $\beta J/k_B = 15.1(2)$ K and $C_2 = 2.86(1)$ cm^3 mol^{-1} K. To check the phase transition behavior of **7**, the curve of $d\log(T)/d\log(\chi_mT)_{ferro}$ vs T was plotted in Supporting Information, Figure S8.[25] Here $(\chi_mT)_{ferro} = \chi_mT - 0.77 \times \exp(-265/T)$ describes the ferromagnetic contribution, which is obtained by subtracting the spin−orbital coupling component that dominates at the high temperature regime from the total χ_mT. A direct fit of the temperatures from 30 to 8 K yields $T_c = 0$ K and $\gamma = \infty$, which is consistent with the theoretical 1D-Ising value (see Supporting Information, Figure S8).[25,26] This behavior may rule out the phase transition to long-range ordering of this system above 0 K and further confirms that **7** is indeed a real 1D system.

Thus, strongly frequency-dependent ac susceptibilities (χ' and χ'' are the real and imaginary components of ac susceptibility, respectively) of **7** below 7 K were observed (Figure 10), which is the typical Ising-type ferromagnetic

(21) Kapoor, R.; Kataria, A.; Venugopalan, P.; Kapoor, P.; Hundal, G.; Corbella, M. *Eur. J. Inorg. Chem.* **2005**, 3884.
(22) Bačo, R. *Coord. Chem. Rev.* **2004**, *248*, 757.
(23) Coronado, E.; Drillon, M.; Nugteren, P. R.; de Jongh, L. J.; Beltrán, D. *J. Am. Chem. Soc.* **1988**, *110*, 3907.
(24) Georges, R.; Borrás-Almenar, J. J.; Coronado, E.; Curély, J.; Drillon M. *One-dimensional Magnetism: An Overview of the Models in Magnetism: Molecules to Materials*, Miller, J. S., Drillon, M., Eds.; Wiley-VCH Verlag: Berlin, 2001; Vol *I*, pp 1−47.
(25) (a) Drillon, M.; Panissod, P.; Rabu, P.; Souletie, J.; Ksenofontov, V.; Gütlich, P. *Phys. Rev. B* **2002**, *65*, 104404. (b) Souletie, J. ; Rabu, P.; Drillon, M. *Scaling Theory Applied to Low Dimensional Magnetic System in Magnetism: Molecules to Materials*; Miller, J. S., DrillonM., Eds.; Wiley-VCH: Weinheim, Germany, 2005; Vol. *V*, pp 347−377.
(26) (a) Widom, B. *J. Chem. Phys.* **1965**, *43*, 3892. (b) Widom, B. *J. Chem. Phys.* **1965**, *43*, 3898.

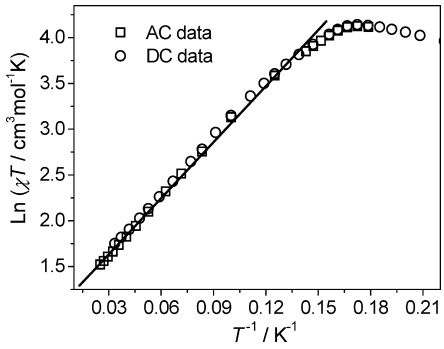

Figure 11. Logarithm of χT vs $1/T$ of **7**. The ac susceptibility was obtained at a frequency of 1 Hz in an ac field of 5 Oe and a zero dc field. The dc susceptibility was obtained in an applied field of 1 kOe. The red line is the result of a fit between 5.6 and 40 K.

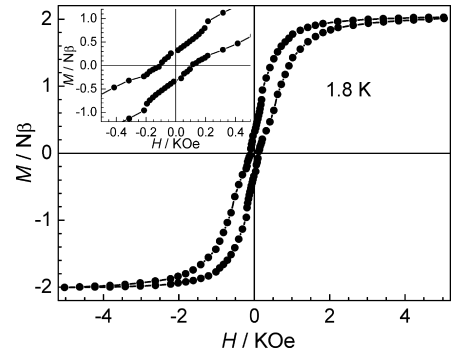

Figure 12. Hysteresis loop of **7** at 1.8 K. Inset: enlarged region in the range of ± 0.5 kOe.

chain behavior predicted by Glauber.[27] The peak temperatures (T_B) of χ'' can be fitted well by the Arrhenius plot extracted from these data, showing the occurrence of a clear crossover between two different activated regimes at $T^* = 4.7$ K ($1/T^* = 0.215$ K^{-1}), and giving the characteristic relaxation time, τ_0, of 3.7×10^{-13} and 1.2×10^{-10} s for the high and low temperature regimes, as well as two corresponding different energy barriers, $\Delta_{\tau 1}/k_B = 109.2$ and $\Delta_{\tau 2}/k_B = 82.1$ K, respectively. This result is similar to the observed finite-size effect[28] halving the Glauber activation barrier in **2**. However, they are both about 29 K larger than those of **2**.

In addition, the peak temperatures (T_p) of χ' can be measured by a parameter $\phi = (\Delta T_p/T_p)/\Delta(\log f) = 0.13$,[29] which is in the range of a normal superparamagnet and precludes the possibility of a spin-glass. Moreover, a shape of the Cole−Cole diagram (inset of Figure 10) can be obtained at 4.5 K, which can be fitted by a generalized Debye model with an α value of 0.23, indicating a narrow-distribution of relaxation time.[30]

The temperature-dependent exponential behavior is evident from the plot of $\ln(\chi T)$ vs $1/T$. Figure 11 shows $\ln(\chi T)$ increasing linearly between 40 and 5.6 K with an energy gap of $\Delta_{\xi 7}/k_B = 20.4(3)$ K and $C_{eff} = 2.78$ cm^3 mol^{-1} K (obtained by fitting the expression $\chi T = C_{eff} \exp(\Delta_\xi/k_B T)$ between 5.6 to 40 K). This value of $\Delta_{\xi 7}/k_B$ is smaller than that of **2** ($\Delta_{\xi 2}/k_B = 24.0$ K). Moreover, from the saturation value of χT, we can estimate the number of spin unit (n) to be about 23, and therefore, the real chain length (L) of the **7** to be about 11.6 nm, which is slightly longer than 10.8 nm of **2** ($C_{eff} = 2.47$ cm^3 mol^{-1} K, $n = 21$).

Below the blocking temperature, the irreversibility effect was observed in **7** with a clear hysteresis loop at 1.8 K (Figure 12) as well as the discrepancy of zero-field-cooled (ZFC) and field-cooled (FC) magnetization at 4.0 K (Supporting Information, Figure S9). The coercive field of the hysteresis loop is 110 Oe, which is similar with that of **2**, confirming a magnet-type behavior. Moreover, the maximum magnetization value of **7** at 2.5 K reaches 2.41 μ_B at 7 T (Supporting Information, Figure S10), which is also similar with that of **2**.

2 and **7** actually have similar SCM behavior except that the obtained energy barrier of **7** is larger than that of **2**. If considering the anisotropic energy barrier, Δ_A, which equals $[\Delta_\tau - 2(\Delta_{\tau 1} - \Delta_{\tau 2})]/k_B$, one gets the result $\Delta_{A7}/k_B = 55$ K $> \Delta_{A2}/k_B = 19.5$ K. Therefore, the reason for the larger Δ_τ of **7** is probably due to the larger Δ_A in **7**, which is actually related to the magnetic anisotropy of Co(II) ions in these two compounds. As is known, the lowest orbital state of the free Co^{II} ion is $^4F_1$. In the weak field of O_h symmetry, the $^4F_1$ term splits into $^4T_{1g}$,$^4T_{2g}$, and $^4A_{2g}$ terms. With reduction of symmetry to D_{4h}, further splitting occurs. First, the $^4T_{1g}$ crystal field term splits into ^4E_g and $^4A_{2g}$, where the ground state, $^4A_{2g}$, can be further splits into Kramers doublets Γ6 and Γ7 when spin orbit coupling is switched on.[16b] The difference between Γ6 and Γ7 states can be written as $2D$.[22] Therefore, the magnetic anisotropy of Co^{II} ions is mainly governed by the crystal field and the spin−orbital coupling terms. Here, we estimated the electrostatic potentials of the metal centers and ligands of **2**, **5**, and **7**, which might explain some of the differences of the crystal field between **2** and **7** (vide infra).

Electrostatic Potential Calculations. To further compare the effect of crystal field, we have also performed electrostatic potential calculations based on Density-Function-Theory (DFT) on **2**, **5**, and **7**. To simplify DFT calculations and give a clear-cut picture, a primitive model of one Co^{II} ion and one deprotonated dicarboxylate ligand was used at the beginning. As shown in Figure 13, the resulting electronic density maps of the three metal−ligand systems are similar, having the positive density all on the Co^{II} ion and negative charge on the carboxylate oxygens. Meanwhile, the optimized carboxylate conformations are different; those in 1,2-chdc and 4-Me-1,2-chdc adopt a similar parallel arrangement, while those in 1,2-chedc feature a perpendicular arrangement owing to the C=C double bond between them. Hence 1,2-chdc and 4-Me-1,2-chdc may lead to similar Co^{II} compounds, while 1,2-chedc probably does not.

(27) Glauber, R. J. *J. Math. Phys.* **1963**, *4*, 294.
(28) (a) Coulon, C.; Clérac, R.; Lecren, L.; Wernsdorfer, W.; Miyasaka, H. *Phys. Rev. B* **2004**, *69*, 132408/1. (b) Bogani, L.; Caneschi, A.; Fedi, M.; Gatteschi, D.; Massi, M.; Novak, M. A.; Pini, M. G.; Rettori, A.; Sessoli, R.; Vindigni, A. *Phys. Rev. Lett.* **2004**, *92*, 207204/1. (c) Bogani, L.; Sessoli, R.; Pini, M. G.; Rettori, A.; Novak, M. A.; Rosa, P.; Massi, M.; Fedi, M. E.; Giuntini, L.; Caneschi, A.; Gatteschi, D. *Phys. Rev. B* **2005**, *72*, 064406/1.
(29) (a) Ma, S. K. *Phys. Rev. B* **1980**, *22*, 4484. (b) Mydosh, J. A. *Spin Glasses: An Experimental Introduction*; Taylor & Francis: London, 1993.
(30) Cole, K. S.; Cole, R. H. *J. Chem. Phys.* **1941**, *9*, 341.

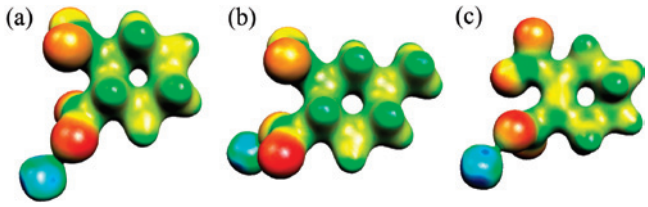

Figure 13. Electrostatic potential mapped on the 0.05 au density isosurface in the M—O from G03/B3LYP for Co(1,2-chdc) (a), Co(4-Me-1,2-chdc) (b), and Co(1,2-chedc) (c). Color codes from blue to red: from +0.6244 to −0.0202 in (a), from +0.6462 to −0.0295 in (b), from +0.6445 to −0.0107 in (c).

Table 3. DFT Results of the Simplest Co(II)-Dicarboxylate Model

	1,2-chdc	4-Me-1,2-chdc	1,2-chedc
Mayer Bond Order of Co—O	0.6135	0.6221	0.6192
Mulliken atomic charge of Co	0.4890	0.4992	0.5265
Mulliken atomic charge of O	−0.5626	−0.5783	−0.5322
Charge difference of Co and O	1.0516	1.0775	1.0587

More importantly, the 4-Me-1,2-chdc-Co^{II} system has the largest electrostatic potential difference between the Co^{II} and carboxylate oxygen, implying the strongest attraction between the Co^{II} and carboxylate among these systems, which is further supported by the Mayer bond order and Mulliken atomic charge difference analyses (Table 3).[31,32] This suggests that a strongest ligand field effect can be found on the energy level of the Co^{II} ion of the 4-Me-1,2-chdc-Co^{II} system.[16,21,22] Electrostatic potential calculations on a more extended model of a four carboxylate-bridged Co^{II} paddle-wheel dimer of 1,2-chdc and 4-Me-1,2-chdc also indicates stronger attraction between the Co^{II} and carboxylates in the 4-Me-1,2-chdc-Co^{II} system (see Supporting Information, Figures S11 and S12 and Table S1), thus further implying that similar results could occur in the fully extended polymeric structures. As some reports show that the *D* value of five-coordinated Co^{II} has an increasing tendency as the ligand field increased,[16] at least we may expect to perturb the magnetic properties of **2** by replacement of 1,2-chdc into the subtly modified analogue 4-Me-1,2-chdc, although a contrary result was observed for Mn^{II} compounds.[33] Therefore, the larger magnetic anisotropy of **7** might be partially due to the stronger ligand field of 4-Me-1,2-chdc. However, an accurate analysis of magnetic anisotropy of Co^{II} ions requires other techniques such as single-crystal magnetism, high-frequency EPR,[2b] inelastic neutron diffraction studies, and so forth.

(31) (a) Mayer, I. *Chem. Phys. Lett.* **1983**, *97*, 270. (b) Mayer, I. *Int. J. Quantum Chem.* **1984**, *26*, 151. (c) Bridgeman, A. J.; Cavigliasso, G.; Ireland, L. R.; Rothery, J. *Dalton Trans.* **2001**, 2095.

(32) (a) Zheng, S.-L.; Messerschmidt, M.; Coppens, P. *Angew. Chem., Int. Ed.* **2005**, *44*, 4614. (b) Zheng, S.-L.; Volkov, A.; Nygren, C. L.; Coppens, P. *Chem.—Eur. J.* **2007**, *13*, 8583.

Conclusions

Five new metal-carboxylate layered compounds containing four kinds of metal−oxygen chains have been hydrothermally synthesized. In these series of magnetic chain-based compounds, only the dimeric paddle-wheel cobalt(II)-carboxylate chain exhibit SCM behavior no matter whether Co^{II} ion coordinates to *trans*-1,2-chdc or 4-Me-1,2-chdc. The presence of SCM behavior in these two Co^{II} compounds is mainly due to (i) the alternating ferromagnetic interactions in the chain, (ii) the Ising-type magnetic anisotropy of Co^{II} ion, and (iii) the very weak interchain magnetic interactions that are achieved by the C—C σ bond and the special steric arrangement of the carboxylates. Although the Fe^{II} *trans*-1,2chdc compound satisfies the last two requirements, the intrachain magnetic interactions are no longer alternating ferromagnetic interactions but alternating ferro- and antiferromagnetic. Therefore, **3** does not exhibit SCM behavior. Other type of chains such as the uniform aqua-carboxylate-bridged Ni^{II} chain in **4**, Co^{II} based Δ-chain in **5**, and the pentanuclear Co^{II} chain in **6** also do not exhibit strong ferromagnetic interactions, and no SCM behavior is observed in these compounds. Although **2** and **7** have very similar SCM behavior, ac magnetic studies show **7** has a higher energy barrier than that of **2**. Such behavior is probably caused by the larger anisotropic energy barrier in **7**.

Acknowledgment. This work was supported by the "973 Project" (Grant No. 2007CB815302 and 2007CB815305), NSFC (Grant No. 20525102) and NSF of Guangdong (Grant No. 04205405). The authors thanks Prof. Marc Drillon (IPCMS, 23 rue du Loess, B.P. 43, 67034 Strasbourg Cedex 2 France) for helpful discussions.

Supporting Information Available: Crystallographic data in CIF file format, additional structural plots, additional magnetic data, and the X-ray diffraction patterns. This material is available free of charge via the Internet at http://pubs.acs.org.

IC801498N

(33) Duboc, C.; Phoeung, T.; Zein, S.; Pécaut, J.; Collomb, M.-N.; Neese, F. *Inorg. Chem.* **2007**, *46*, 4905.